CI&CEQ
Chemical Industry & Chemical Engineering Quarterly

Available on line at
Association of the Chemical Engineers of Serbia *AChE*
www.ache.org.rs/CICEQ

Chem. Ind. Chem. Eng. Q. 25 (4) 353–360 (2019) CI&CEQ

M. DRAMICANIN[1]
S. BALOS[1]
P. JANJATOVIC[1]
I. ZABUNOV[2]
V. GRABULOV[3]

[1]Department of Production Engineering, Faculty of Technical Sciences, University of Novi Sad, Novi Sad, Serbia
[2]Faculty of Special Technology, Alexander Dubček University of Trenčín, Trenčín, Slovak Republic
[3]Institute IMS, Belgrade, Serbia

SCIENTIFIC PAPER

UDC 621.791:669.14.018.8

ACTIVATED FLUX TIG WELDING OF STAINLESS-STEEL PIPES

Article Highlights

- 20 nm TiO_2 nanoparticles proved effective in increasing the penetration
- Activated flux is effective when combined with pulse current orbital TIG welding
- The applied activated flux is effective with pulse current and without consumable material
- Weld properties obtained with the activated flux comply with relevant standards

Abstract

In this work, the presence of TiO_2 nanoparticle-based activated flux combined with orbital welding of seamless thick-walled pipes of stainless steel and low-cycle pulse current was done, representing a novel combination of welding processes parameters. Control specimens were welded without flux and consumable material, and without flux with the consumable material. Experimental welding with different welding parameters was done. Special attention was given to characterize the flux by zetasizer method, representing a new approach, versus the conventional approach where the nominal oxide particle size is reported. The obtained welds were visually tested, macroanalyzed, their microstructures examined, and their tensile and bending properties determined. The results show that the flux influences a significant increase in penetration depth, up to full penetration, which has a positive effect on the increase in the tensile and bending properties of the weld metal. Material beahvior model was developed, based on microstructural features of the near weld-line. Without the flux, grain enlargement occurred near the surface, while with flux, it occurred under the weld, which can be attributed to recrystallization and a reversed Marangoni convection.

Keywords: orbital welding, oxide coating, mechanical properties, depth of welding.

Welding is a technology that makes the joining of two, or more, similar or dissimilar materials. The welded joint can be made with or without consumable material [1]. Recently, special welding procedures have been developed that enable the welding of special materials in different, specific conditions. One of the special procedures described in this paper is the process of orbital welding, which uses GTAW - gas tungsten inert welding or TIG - tungsten inert gas welding with pulse current [2]. The process is automated and gives the highest quality of the weld metal. Orbital welding is used for welding pipes for pipelines in the food and pharmaceutical industries as well as for the gas and petrochemical industries [3].

To improve the TIG welding active flux, A-TIG was developed. The application of flux in TIG was proposed for the first time in the 1960s by Paton Welding Institute of National Academy of Sciences, Ukraine, by Gurevich *et al.* [4]. In this welding process, a thin layer of flux is applied with a brush or sprayed over the prepared surface to be welded. Fluxes were fabricated by mixing, usually metallic oxide powders with solvents, most frequently acetone and ethanol [5-9]. In the A-TIG process, penetration is increased, a lower electric energy consumption is achieved, no V-preparation and consumables are

Correspondence: M. Dramicanin, Department of Production Engineering, Faculty of Technical Sciences, University of Novi Sad, Novi Sad, Serbia
E-mail: dramicanin@uns.ac.rs
Paper received: 29 December, 2018
Paper revised: 18 March, 2019
Paper accepted: 6 April, 2019

https://doi.org/10.2298/CICEQ181229013D

needed. As a result, this process offers a low cost and is time-saving [10-17]. In accordance to the results obtained by Modenesi *et al.* and Dong *et al.,* the increase in weld penetration can be attributed to the reversal of the Marangoni convection [11,18]. The Marangoni convection is a surface tension-driven convection depending on the surface tension gradient in the fluid: fluids flow from areas where surface tension is lower towards areas where it is higher, which is the case with conventional TIG. The reversed Marangoni convection in A-TIG influences the molten metal to flow towards the center of the weld and to the bottom of the weld, causing a narrower, but deeper weld. Another effect is the arc constriction influenced by the presence of electronegative elements such as Si and Ti, as reported by Skvortsov and Tanaka *et al.* [19,20]. Tseng and Lin [2] used these concepts and achieved depth-to-width ratios of 1.08 in UNS S31603 stainless steel. Vora and Badheka [21] tested fluxes based on Al_2O_3, Co_3O_4, CuO, HgO, MoO_3 and NiO on ferritic/martensitic steel. Of these, the most effective were Co_3O_4 and CuO. Venkatesan *et al.* [22] studied the effect of SiO_2, TiO_2 and Cr_2O_3 in different ratios, finding the mixtures of powders to be superior compared to single component fluxes on AISI 409 ferritic stainless steel. Vora and Badheka [21] tested micro- and nanoparticle-based fluxes. They found that particle size of Al_2O_3 does not have a significant influence on penetration, unlike SiO_2. Also, there have been several attempts to mathematically predict the A-TIG process [23].

The aim of this paper is to investigate the oxide-based coating to increase the penetration depth in orbital welding of thick-walled austenitic stainless-steel pipes, by using TiO_2 nanoparticle-based flux.

EXPERIMENTAL

The base metal used for welding was AISI 304 (X5CrNi18-10) stainless steel in the form of pipes, with the external diameter of 72 mm and wall thickness of 5.2 mm. The chemical composition of this material was as follows: 0.05% C, 1% Si, 1.6% Mn, 17.73% Cr, 0.01% P, 0.01% Al, 0.3% Cu, 9.7% Ni, 0.2% Mo, 0.01% Sn, 0.05% V, balance Fe. Mechanical properties of the pipe were: proof strength R_e = = 280 MPa, ultimate tensile strength R_m = 624 MPa and elongation A = 65%. These pipes were cut to the length of 80 mm using an Orbitec ORS 115 cutting saw. After that, the pipes were cleaned with ethanol. Afterwards, manual TIG tack welding was performed.

Before welding, the coating was prepared and based on a 15% TiO_2 20 nm nanoparticle solution in ethanol. The size of the particles in the liquid component was determined by Zetasizer Nano ZS analyzer, Figure 1. The coating, having a width of 20 mm was applied by a 10 mm brush. Shortly before mounting of the pipes into the orbital device clamp, both their ends were sealed with aluminum tape. Then, two holes were drilled, one for the hose blowing protective gas (argon), while the other was used to place the probe of an oxygen analyzer (Oxy Integral) to measure oxygen content in a protective atmosphere of argon. The probe was inserted into the two-pipe butt weld assembly. An Orbitec OSW 115 open orbital welding head was used, coupled to an EWM Tetrix 200 welding device. After setting and fixing the welding head, the adjustment of the distance between the electrode and the pipe surface was done. The welding was done with a 2.4 mm tungsten-2% thoriated electrode with a tip angle of 90°. Pipes were welded without any root opening.

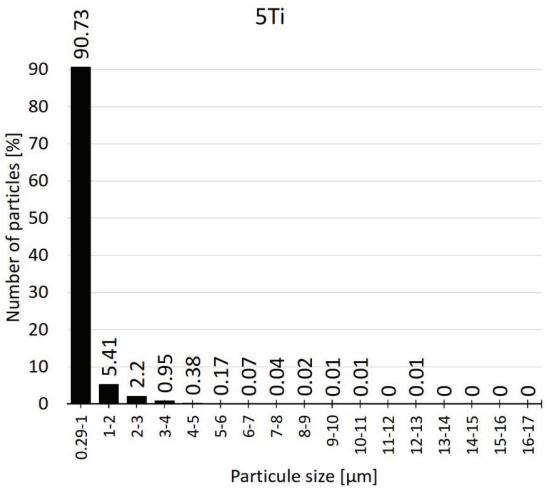

Figure 1. Particle size distribution in the solvent.

Experimental welding was carried out on seven samples, on five samples with applied flux (samples 1-5) and without consumable material. The welding of the first sample (0) was carried out without coating, while the welding of the last sample (6) was carried out without an oxide flux but using a consumable material. The consumable wire was MIG 19/9 ER308LSI, produced by Elektrode Jesenice, with 0.8 mm diameter and the following chemical composition: ≤0.02% C, 1.95% Mn, 0.8% Si, 20.0% Cr, 10.0% Cr, balance Fe.

Welding parameters are shown in Table 1, with changed parameters depicted in bold. These parameters were calculated automatically based on the diameter and thickness by Orbitec TIGTronic. It should be noticed that welding sectors were as shown

Table 1. Welding parameters

Parameter		Specimen No.						
		0	1	2	3	4	5	6[a]
Primary (peak) current I_1 [A]	Sector 1				175			
	Sector 2				170			
	Sector 3				165			
	Sector 4				160			
Background current I_2 [A]	Sector 1-4				53			
Primary current time [s]		1.59	1.59	1.59	1.59	1.20	1.40	1.59
Background current time [s]					1.59			
Welding speed primary current I_1[mm/min]					0			
Welding speed background current I_2[mm/min]					100			
Current ramp down time-downslope time [s]		30	30	5	30	30	30	30
Oxygen content in the atmosphere [ppm]					<20			
Pre/post gas time [s]					3/5			
Torch gas flow [l/min]					12			
Purge gas flow [l/min]		10	10	10	7	10	10	10

[a]Welding wire feeds speeds for I_1 and for I_2 were 400 and 200 mm/min, respectively

in Figure 2: sector 1 from 12 to 3 o'clock (0-90°); sector 2 from 3 to 6 o'clock (90-180°), sector 3 from 6 to 9 o'clock (180-270°) and sector 4 from 9 to 12 o'clock (270-360°/0°).

After welding, the test procedure was performed in accordance to standard EN ISO 15614. Characterization techniques used were as follows: the non-destructive technique (visual testing) and the destructive techniques, mechanicals testing (tensile, bending) and macro metallographic tests. Specimens were cut perpendicular to the weld on locations as shown in Figure 2.

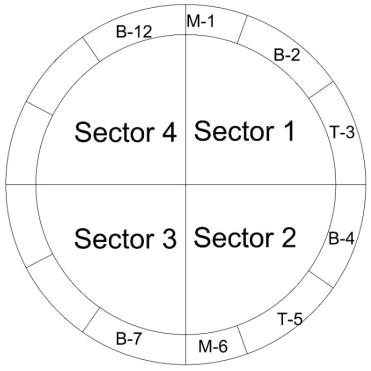

Figure 2. The Schematic representation of the specimen locations for: M – macro and hardness test, T- tensile test, B – bending test.

Weld measurements were done by standard gauges in the most sensitive positions between sectors 4 and 1 (top position M-1) and between the 2nd and 3rd sector (bottom position M-6). On these positions, excess weld metal and root concavity had a maximum or minimum value. The metallographic examination was done after standard preparation procedure: grinding with sandpapers, polishing and etching with aqua regia (10 ml HNO_3, 25 ml HCl and 20 ml glycerine) and examination by Leitz Orthoplan light microscope. Tensile testing and band testing were preformed on a WPM ZDM 5/91 tensile testing machine. Tensile specimens T3 and T5 were machined according to EN ISO 4136 with 12 mm width. The bend testing was done on four specimens per sample, one from each sector, two for face bend tests and two for root bend tests. Bending specimens were machined to 15 mm width, according to EN ISO 5173, also with removed excess weld metal. The bend test to maximum bending angle of 180° was performed with a 20 mm diameter plunger with the distance between the supports being 30.5 mm.

RESULTS AND DISCUSSION

Macro-testing and penetration depth

The results of a macro test of the represented specimen, along with the penetration depth indicated, are shown in Figures 3 and 4. In Figure 3, macro images of welds in the top position, while in Figure 4, macro images of welds in the bottom position, are shown. It can be seen that specimens welded without the flux clearly do not offer full penetration, the penetration reaching around the half of the pipe wall thickness. In specimens welded with the flux, different weld profiles can be observed, mainly having near-parallel melting lines (specimens 1-3) and nearly V-shaped (specimens 4 and 5). On the other hand,

macro images of welds in the bottom position are shown in Figure 4. Specimens welded without the flux had a similar profile, however, specimens 4 and 5 clearly had lower penetration in the bottom versus the top position. On the other hand, specimen 6, welded with the consumable material, showed slightly higher penetration than in the top position. In all specimens, a typical columnar morphology can be observed.

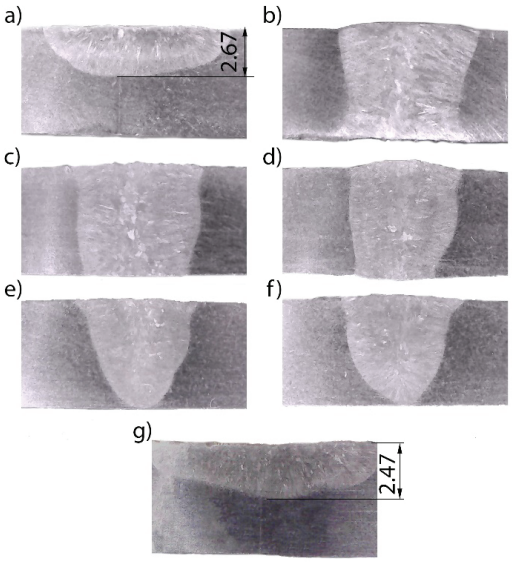

Figure 3. Macro-images of welds in the top position of the pipe.

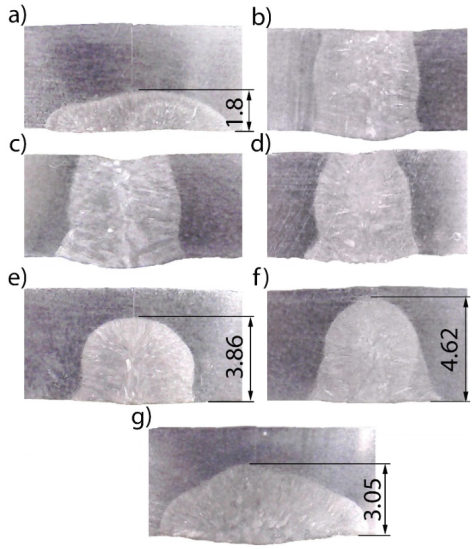

Figure 4. Macro-images of welds in the bottom position of the pipe.

Weld metal measurements

Weld metal measurements are shown in Table 2. Sample 2 had maximum excess weld metal at the top position while samples 1 and 3 had maximum excess weld at the bottom position.

Table 2. Weld measurements

Sample	Top position		Bottom position	
	Excess weld metal	Root concavity	Excess weld metal	Root concavity
0	0.65	No penetration	0.30	No penetration
1	-0.65	-1.80	0.60	+0.05
2	0.80	+0.05	0.60	+0.35
3	0.75	-1.8	0.80	+0.3
4	0.80	No penetration	0.70	No penetration
5	0.55	+0.50	0.10	No penetration
6	0.15	No penetration	0.50	No penetration

According to the standard ASME BPE-2014 – Bioprocessing Equipment, which is used on the welding pipes in the pharmaceutical industry, root concavity of the welded joint can be up to 10% of the wall thickness of the pipe, that is, for this pipe wall thickness of 0.52 mm. The maximum measured depth of root concavity is 0.35 mm for sample 2, which means that samples 1, 2 and 3 satisfy this criterion (Table 2). During welding, when the welding head passes over the bottom position, the melt material from the outside forms the excess weld metal, while due to the lack of melt material on the inside, root concavity forms.

Apart from specimens welded without the flux (0 and 6) and specimens where the parameters allowed full penetration in both positions (specimens 1-3), specimens 4 and 5 may be of interest due to non-full penetration in one or both tested positions. In specimen 4, primary current time was reduced, causing an insufficient penetration both in top and bottom positions. On the other hand, in specimen 5, where a primary time was partially recovered, but still not to the level of specimens 1-3, the full penetration was achieved only in the top position, however, in the bottom position, no full penetration was achieved (Figures 3 and 4).

Metalographic examination

Microstructures in the weld joint are shown in Figures 5 and 6, in the bottom position. In Figure 5, microstructures near the weld melt line close to the specimen surface are presented. Also, the dendrite weld metal microstructure is shown, present in both specimens, the result of the solidification process that occurs after the tungsten-based electrode passes over the material. It can be seen that austenitic grains in specimen 0 are larger than those in specimen 4, which is marked by arrows. On the other hand, micro-

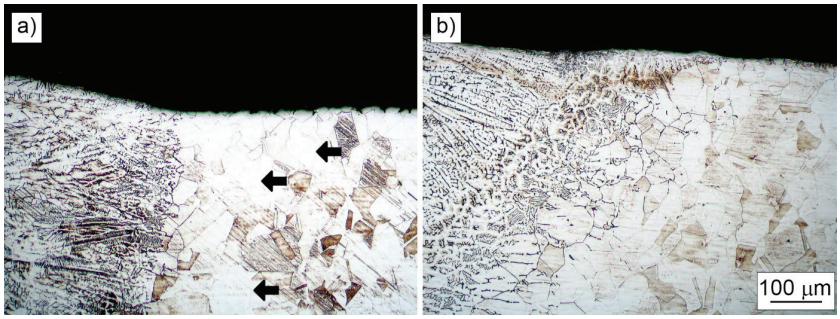

Figure 5. Microstructures near weld melt line close to the specimen surface: a) specimen 0; b) specimen 4.

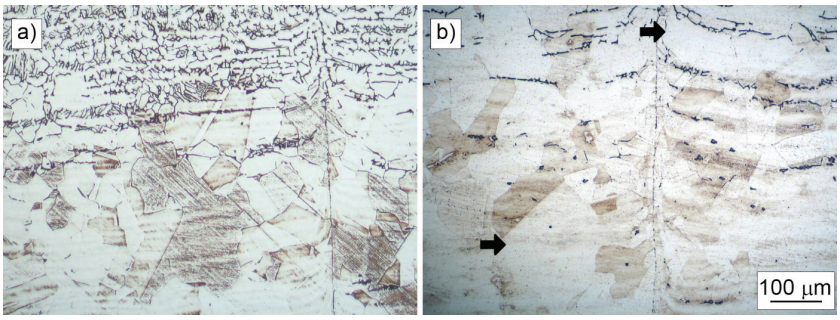

Figure 6. Microstructures near weld melt line under the weld: a) specimen 0; b) specimen 4.

structures under the weld, near the melt line, show different behavior. Namely, enlarged grains are present in specimen 4, as marked by arrows.

Tensile testing results

The results of tensile testing for two sections: T-3 (designated as -1) and T-5 (designated as -2) of all samples are shown in Table 3, in as-welded conditions.

Table 3. Results of tensile testing; failure location: weld metal

Sample	Tensile strength R_m [MPa]
0-1	260
0-2	331
1-1	581
1-2	582
2-1	597
2-2	584
3-1	573
3-2	594
4-1	472
4-2	438
5-1	564
5-2	533
6-1	371
6-2	427

Based on the results shown in Table 3, it can be seen that the highest value of tensile strength was obtained during welding when the oxide coating was present. The lowest value of tensile strength was obtained for sample 0 without the oxide coating during welding, since the penetration was the lowest, proved by weld dimension measurements and macro imagery. In all specimens, the fracture occurred in the weld metal.

Results of bend testing

The results of bend testing are shown in Table 4 and Figure 7. No sample developed a crack when bent over the weld face. When the specimens were

Table 4. Bending test results

Sample	Sector	Bend over	Observation
0	1, 2	Face	Pass
	3, 4	Root	Fail
1	1, 2	Face	Pass
	3, 4	Root	Pass
2	1, 2	Face	Pass
	3, 4	Root	Pass
3	1, 2	Face	Pass
	3, 4	Root	Pass
4	1, 2	Face	Pass
	3, 4	Root	Fail
5	1, 2	Face	Pass
	3, 4	Root	Pass
6	1, 2	Face	Pass
	3, 4	Root	Fail

examined over the root, some of them developed a crack or opened but did not fully fractured. This was expected since in some samples no full penetration was achieved: samples welded without oxide coating (0 and 6), as well as welded with the oxide coating in sample 4.

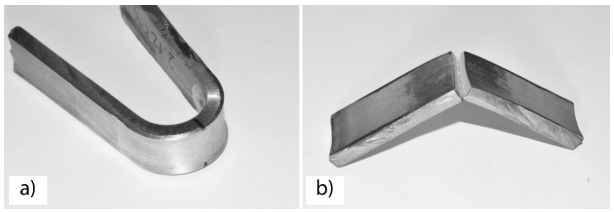

Figure 7. Bend testing results of specimen: a) sample 1, sector 2 (B-4), without fracture; b) sample 6, sector 3 (B7), with fracture.

When bending over the root of the weld metal, the situation is different because, as can be seen from Table 4 for samples 0, 4 and 6, the test is not satisfied, *i.e.*, there was a sample opening. The samples in which no full penetration was achieved did not pass the bending tests. Also, the results of the bend test are in agreement with tensile test results, both being inadequate.

Material behavior model and weld effectiveness

The material behaviour model is shown in Figure 8. Enlarged grains near the surface in the specimen welded without the flux and under the weld in the specimen welded with the flux is the result of different molten metal flow when the weld is performed without and with the flux. This is proving theoretical explanations of an increased penetration with A-TIG. Enlarged grains generally appear due to recrystallization, that is, increased heat transfer from the weld pool towards the base metal. In specimen 0, obviously, the heat is transferred more intensively towards weld surface, meaning the flow is from the weld centre towards the melt lines. When the molten metal starts to flow downwards, it had already passed its heat to the base metal. In specimen 4, the flux causes the reversal of the material flow (reversal of Marangoni convection) and the recrystallization occurs at the bottom of the specimen. When the flow reaches the sides, the molten metal has already given much of its heat.

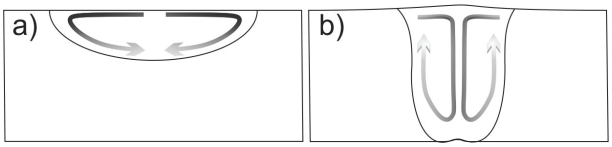

Figure 8. Material behavior model: a) without the flux; b) with the flux.

Samples welded using an oxide coating have a tensile strength two times higher than the samples welded without coating. The important fact is that in the samples welded with the application of the oxide coating, the tensile strength is similar. The depth of penetration has an important influence on the result of tensile testing. Weld efficiencies in samples 1, 2 and 3 was over 90% of the tensile strength of the base metal (Figure 9). Samples 4 and 5 have a lower efficiency, due to non-optimal shortened primary current time.

The approach shown in this study offers several novelties. A very fine 20 nm nano TiO_2-based flux was used in combination with an automatic orbital welding device aimed at welding pipes. The application of a zetasizer particle distribution test proved that the smallest particles present in the flux are of between 0.29 and 1 μm size, proving that there is a significant agglomeration present. Finally, the combination of A-TIG welding with low cycle pulse current used in orbital welding is not conventional.

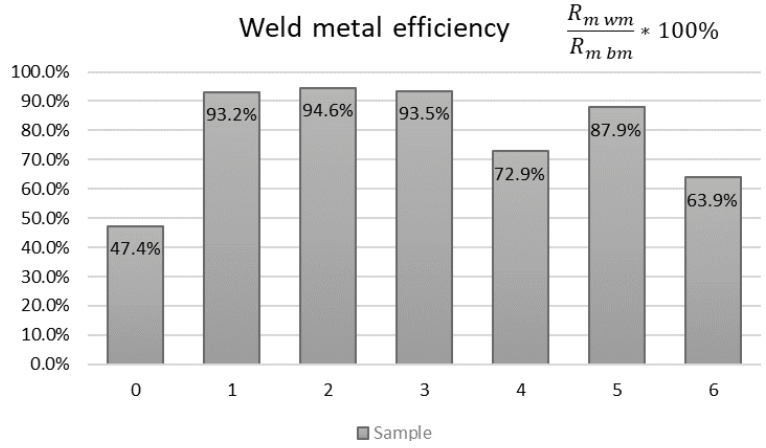

Figure 9. Weld metal efficiency.

CONCLUSIONS

Based on the results, the following conclusions can be drawn:

- By adding the oxide coating in orbital welding, the weld metal shape changes due to the effect of the Marangoni effect. The results of the Marangoni effect are the increasing of depth of penetration for more than 100% compared to welding without the oxide coating, while at the same time significantly reducing the width of the weld metal.
- A-TIG flux containing TiO_2 nanoparticles do not have an adverse effect on the mechanical properties of the weld metal. After welding, weld metal effectiveness reaches 94% of the tensile strength of the base metal
- The optimized orbital welding technology can be used to weld austenitic steel pipes with weld dimensions complying with ASME BPE-2014 – Bioprocessing Equipment.
- A-TIG based on TiO_2 nanoparticles can be used to enhance the performance of orbital low-frequency TIG pulse welding.

Acknowledgments

The authors gratefully acknowledge research funding by the project “Development and Application of Advanced Characterization of Materials and Welds in Production Engineering” of the Department of Production Engineering, Faculty of Technical Sciences Novi Sad, Serbia.

REFERENCES

[1] K.-H. Tseng, C.-Y. Hsu, J. Mater. Process. Technol. 211 (2011) 503-512

[2] K.-H. Tseng, P.-Y. Lin, Materials 7 (2014) 4755-4772

[3] F. Baumbach, in Hygiene in Food Processing Principles and Practice, H.L.M. Lelieveld, M.A. Mostert, B. White, J. Holah Eds., Woodhead Publishing, Cambridge, 2014, pp. 179-196

[4] S.M. Gurevich, V.N. Zamkov, N.A. Kushnirenko, Avtom. Svarka 9 (1965) 1-4

[5] H.-Y. Huang, Metall. Mater. Trans., A 41 (2010) 2829--2835

[6] T. D. Paskell, US5804792A (1996)

[7] K.-H. Tseng, N.-S. Wang, US20160167178A1 (2016)

[8] V. Muthukumaran, A.K. Bhaduri, B. Raj, US8097826 (2010)

[9] K.H. Dhandha, V.J. Badheka, Mater. Manuf. Processes 17 (2015) 48-57

[10] S.G. Nayee, V.J. Badheka, Mater. Manuf. Processes 16 (2014) 137-143

[11] P.J. Modenesi, E.R. Apolinário, I.M. Pereira, J. Mater. Process. Technol. 99 (2000) 260-265

[12] H.-L. Lin, T.-M Wu, Mater. Manuf. Processes 27 (2012) 1457-1461

[13] S. Kou, Welding metallurgy, 2nd ed., Wiley – Interscience, New York, 2003, pp. 116-117

[14] M. Vasudevan, A.K. Bhaduri, B. Raj, K.P. Rao, Mater. Manuf. Processes 22 (2007) 641-649

[15] N. Chandrasekhar, M. Vasudevan, Mater. Manuf. Processes 25 (2010) 1341-1550

[16] V. Maduraimuthu, M. Vasudevan, V. Muthupandi, A.K. Bhaduri, T. Jayakumar, Metall. Mater. Trans., B 43 (2012) 123-132

[17] T. Sakthivel, M. Vasudevan, K. Laha, P. Parameswaran, K.S. Chandravathi, S. Paneer-selvi S, V. Maduraimuthu, M.D. Mathew, Mater. Sci. Eng., A 591 (2014) 111-120

[18] C. Dong, Y. Zhu, G. Chai, Aeronaut. Manuf. Technol. Suppl. 6 (2004) 271-278

[19] E.A. Skvortsov, Weld. Int. 12 (1998) 471-475

[20] M. Tanaka, T. Shimizu, T. Terasaki, M. Ushio, F. Koshiishi, C.-L. Yang, Sci. Technol. Weld. Joining 5 (2000) 397-402

[21] J.J. Vora, V.J. Badheka, J. Manuf. Process. 20 (2015) 224-233

[22] G. Venkatesan, J. Goeuge, M. Sowmyasri, V. Muthapandi, Procedia Mater. Sci. 5 (2014) 2402-2410

[23] P.S. Rao, O.P. Gupta, S.S.N. Murty, A.B.K. Rao,Int. J. Adv. Manuf. Technol. 45 (2009) 496-505.

M. DRAMICANIN[1]
S. BALOS[1]
P. JANJATOVIC[1]
I. ZABUNOV[2]
V. GRABULOV[3]

[1]Departman za proizvodno mašinstvo, Fakultet tehničkih nauka, Univerzitet u Novom Sadu, Novi Sad, Srbija
[2]Faculty of Special Technology, Alexander Dubček University of Trenčín, Trenčín, Slovak Republic
[3]Institut IMS, Beograd, Srbija

NAUČNI RAD

ZAVARIVANJE CEVI OD NERĐAJUĆEG ČELIKA TIG POSTUPKOM SA AKTIVNIM PREMAZOM

U ovom radu, izvršeno je ispitivanje uticaja premaza baziranog na TiO_2 nano-česticama, kombinovanog sa orbitalnim zavarivanjem bešavnih cevi od nerđajućeg čelika sa primenjenom niskocikličnom strujom zavarivanja, što predstavlja inovativnu kombinaciju parametara zavarivanja. Kontrolni uzorci su zavareni sa premazom, bez premaza i bez premaza sa upotrebom dodatnog materijala. Izvršeno je eksperimentalno zavarivanje sa različitim parametrima zavarivanja. Posebna pažnja je posvećena karakterizaciji premaza upotrebom uređaja zeta sizer, što predstavlja potpuno nov pristup, u odnosu na konvencionalni pristup prikazivanja nominalne veličine čestica. Dobijeni zavareni spojevi su ispitani vizuelno, izvršeno je makro-ispitivanje, ispitane su mikrostrukture, kao i ispitivanje zatezanjem i savijanjem. Ispitivanja su pokazala da primenjeni premaz značajno povećava dubinu uvara, sve do pune penetracije, što ima pozitivan efekat na povećanje zateznih i savojnih karakteristika metala šava. Na osnovu dobijenih rezultata metalografskih ispitivanja zone neposredno pored linije topljenja, dat je model toka tečnog metala. Bez premaza, uvećanje austenitnog zrna se javlja neposredno ispod površine osnovnog materijala, dok se sa premazom, uvećanje zrna pojavljuje ispod metala šava, što je može pripisati rekristalizaciji i promeni smera Marangonijeve konvekcije.

Ključne reči: orbitalno zavarivanje, oksidni premaz, mehaničke osobine, dubina uvara.